

Vp/Vs and AVO analysis used in monitoring heavy-oil cold production

Duojun A. Zhang and Larry R. Lines

ABSTRACT

Vp/Vs and AVO analysis were researched to monitor the recovery process of heavy-oil cold production in this paper. Reference horizons were selected based on synthetic seismograms and interpreted on 3D PP and PS seismic volumes. The target formation is surrounded by picked reference top and bottom horizons. To enhance the similarity of PP and PS seismic volumes, a band-pass filter was designed based on the frequency spectrum of PS volume and applied to the PP seismic volume. *Vp/Vs* calculated from PS and filtered PP seismic volumes were compared with that from PS and unfiltered PP seismic volumes. The primary result is encouraging and further research should be done to reveal the direct effect of heavy-oil cold production on *Vp/Vs*. Meanwhile, AVO modeling was done for one oil well based on fluid substitution modeling. In unconsolidated sand reservoirs, cold production of heavy-oil will create a typical Class III AVO response. The indicator A*B (intercept*gradient) value of post-production from the pay zone is obviously distinguished from other cases.

INTRODUCTION

Cold production of heavy oil is a non-thermal process, in which sand and oil are produced simultaneously. This process has been economically successful in several heavy oil fields in Alberta and Saskatchewan. The extraction of sand creates a wormhole network and a foamy oil drive. These two effects are thought to be the main influences in enhanced oil recovery. Commencement of cold production disturbs the initial reservoir state through the presence of foamy oil and wormholes, modifying the fluid phase and elastic properties within drainage areas. Table 1, provided by Alberta Research Council, shows the in-situ reservoir parameters from a 3-year old cold production well in the Lloydminster field. The main changes in the reservoir are the pressure dropping from 3MPa to 1.5MPa, the oil saturation decreases by 10% to 70%, and the gas saturation increases to 10% from non-gas in the initial reservoir. The effects of foamy oil and wormholes have been calculated by Sandy Chen and the results are given in table 2 and Figure 1 (Chen, 2004). Table 2 contains the physical and seismic properties of reservoir rock in the drainage regions with foamy oil effect before and after production. With a 10 percent gas saturation, the average bulk modulus of the saturated rock drops dramatically from 10.6GPa to 7.8GPa due to production, the average P-wave velocity decrease from 2795m/s to 2570m/s. Figure 1 shows that when the wormhole density is less than 14%, the *Vp/Vs* of the drainage region has a gas-dominated *Vp/Vs*, lower than the initial reservoir state. Figure 2 is the crossplot of *Vp/Vs* calculated from fluid substitution results based on Biot-Gassmann's equation for pre- and post-production. The *x*-axis represents post-production and the *y*-axis represents pre-production. The fact that all the points are above diagonal line $y=x$ means a decrease of *Vp/Vs* due to production in practical situation. All of the above tell us that we might be able to use *Vp/Vs* and AVO analysis to monitor the recovery process of heavy-oil cold production.

In this paper, the distribution of V_p/V_s was calculated from 3D PP and PS seismic data; the AVO model for the well 01/1-6/0 was built up from the fluid substitution calculations based on the Biot-Gassmann's equation. Both methods proved to be efficient methods for monitoring heavy-oil cold production.

Table1. In-situ reservoir parameters of a 3-year old cold production reservoir

Parameters	Pre-production	Post-production
Heavy-oil API	11.3	11.3
Specific gravity of methane	0.56	0.56
Solution gas-oil ratio	7.5	7.5(6)
Reservoir temperature(°C)	20	20
Reservoir pressure(MPa)	3	1.5
Water saturation(%)	20	20
Oil saturation(%)	80	70
Gas saturation(%)	0	10
Water salinity(ppm)	44000	44000

Table 2. Seismic properties of drainage sands with foamy oil effects

Physical properties	Pre-production	Post-production		
	Sg=0, So=0.8	Reuss	Voigt	Average
Saturated rock bulk modulus (GPa)	10.616	5.2252	10.113	7.807
Saturated rock shear modulus (GPa)	4.6726	4.6777	4.6777	4.676
Saturated rock bulk density (kg/m ³)	2156.5	2126.6	2126.6	2126
Vp (m/s)	2795	2325	2773	2570
Vs (m/s)	1472	1483	1483	1483

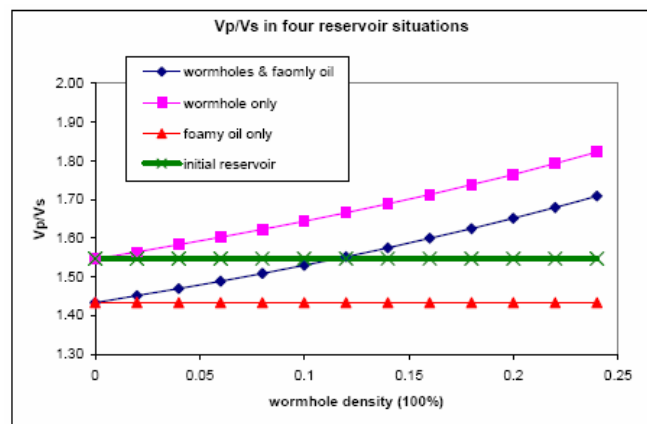


FIG. 1. Comparisons of V_p/V_s in four reservoir situations.

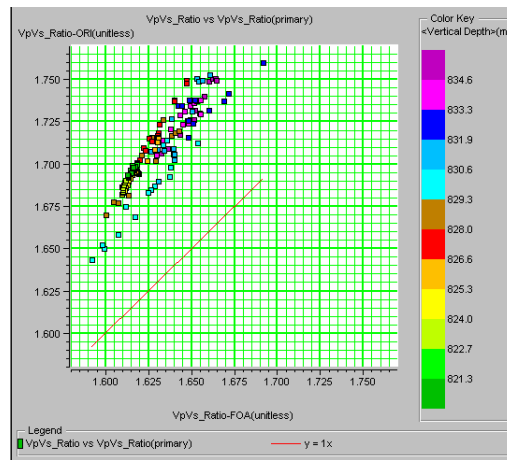


FIG. 2. Crossplot of Vp/Vs between pre- and post-production.

DATA

To research the influence of foamy oil and wormholes on the physical properties, a vertical (PP) 3D data and a radial (PS) 3D data, from the Plover Lake field, were interpreted using Hampson-Russell software. More than 40 wells have already been drilled to develop heavy-oil in an area of about 8.2 km² (Figure 3). Detailed information is not available yet, but hands-on data is enough to give us a preliminary idea about the change in physical properties due to heavy-oil cold production. The 3D seismic data was composed of 145 in-lines and 282 cross-lines with a bin size of 20X10 meters. The PP seismic data revealed wave fields of incident P-wave and reflected P-wave; at the same time, PS seismic data recorded the wave fields of incident P-wave and reflected S-wave. Based on the interpretation of the top and bottom horizons of our target formation on both PP and PS 3D seismic data, we can calculate the Vp/Vs of the target formation based on equation (1) to monitor the disturbance of Vp/Vs deduced by the heavy-oil cold production. Comparing the location of the drilled wells with the distribution of Vp/Vs , we could probably find some correspondence between them. If there is some discernible correlation between the disturbance of Vp/Vs and the process of heavy-oil cold production in the real data, multicomponent seismic data will then be able to play a role in monitoring the process of heavy oil cold production. Applications of this method to heavy-oil reservoirs have been shown by Watson et al. (2002) and Lines et al. (2005).

$$\frac{v_p}{v_s} = \frac{2\Delta t_{ps} - \Delta t_{pp}}{\Delta t_{pp}} \quad (1)$$

Where Δt_{pp} is the travel time of the interpreted interval from PP sections and Δt_{ps} is the internal travel time from PS sections.

There are 9 wells available in the area with both P-wave sonic and density well log data, including 3 wells with S-wave sonic well log data. Due to the low reliability of S-wave sonic data, a conventional fluid substitution technique based on P-wave and density

well log data was used. Well log data from oil well 01/1-6/0 were selected to do AVO modeling, as shown in the later part of this paper.

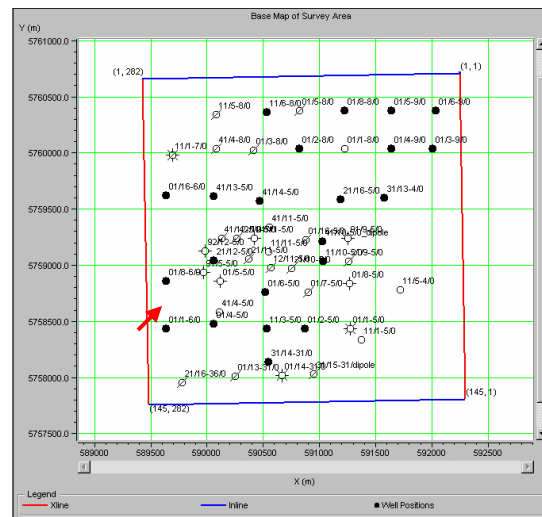


FIG. 3. Basemap of the project.

INTERPRETATION OF SEISMIC DATA

Firstly, the synthetic seismograms were created for both PP and PS seismic data based on the P-wave and S-wave sonic data from well 31/15-31/dipole (Figures 4 and 5). The Bakken formation is the producing heavy-oil layer in this project and the thickness of the layer is about 20 meters. Generally, it's difficult to resolve reflections from the top and bottom of the target layer in the real seismic data, especially in the PS seismic data or the reflected events from the top and bottom of the pay zone are incoherent and difficult to pick. In this case, we will have to select the reference top and bottom horizons to pick, which surrounds our target formation. If the interpreted interval between picked top and bottom horizons is thicker than the actual target layer, the calculated V_p/V_s will be smeared or affected by its surrounding layer. The error analysis will be discussed in the later part of this paper. On the other hand, the exactness and consistency of the picked reflections from the top and bottom of the layer in both PP and PS seismic data are the basis for the V_p/V_s calculations. Finally, we should make a balance between the exactness of the interpreted horizons and the closeness of the picked horizons to the reflections from the top and bottom of the target formation. The criteria for selecting the reference top and bottom horizons are: (1) they should be coherent events across all over the seismic volume to guarantee exactness; (2) they should correspond to same reflecting geologic boundaries for both PP and PS data sets; (3) they should be as close as possible to the reflections from the top and bottom of the target formation to reduce the smearing effect.

According to above criteria, the final reference top and bottom horizons in both PP and PS synthetic seismograms were selected and they are plotted together in Figure 6, including P-wave and S-wave sonic log. In Figure 6, both PP and PS sections are

displayed in the P-P time scale. The PS section was converted to the PP time scale according to the correlation of the corrected P-wave and S-wave sonic data after correlating both PP and PS synthetic seismograms with corresponding real seismic data. Actually, the PP section can be displayed in the PS time scale also by a similar conversion. From Figure 6, we can see that the selected reference horizons correspond with each other very well between the PP and PS sections.

Figures 7 and 8 show the amplitude spectra of PP and PS seismic data respectively. They are quite different. The frequency band of PP spectrum is wider than that of the PS spectrum and the dominant frequency of PP data is also much higher. In the real geological model, layers with similar lithology, are usually very thin and are interbedded with each other. Two corresponding picked horizons (usually the peaks of the events) from the two seismic volumes (acquired in the same area) with different frequency band are probably reflected from different impedance interfaces due to the filtering effect of the thin layers, even though they are apparently similar on both seismic volumes. Therefore, a band pass filter was applied to the PP seismic data, which had a wider frequency band and higher dominant frequency. The band filter was designed based on the frequency spectrum of the PS seismic data, which has a narrower frequency band and a lower dominant frequency. Figure 9 shows the frequency spectrum of PP seismic data after applying the designed band filter. It is similar to the spectrum of PS seismic data. Comparing original PP and filtered PP data (Figure 10), we can see the difference of the event character between them. Also from Figures 11 and 12, we can see that PS seismic data matches better with the filtered PP data compared to the unfiltered PP data. Figure 13 displays the difference of the top horizons between the unfiltered and filtered PP data. Figure 14 reveals the difference of the interpreted interval isochron maps between the two. The actual differences are not so prominent, just several milliseconds difference, but they will play some effect on the final pattern of Vp/Vs , especially in some detailed areas.

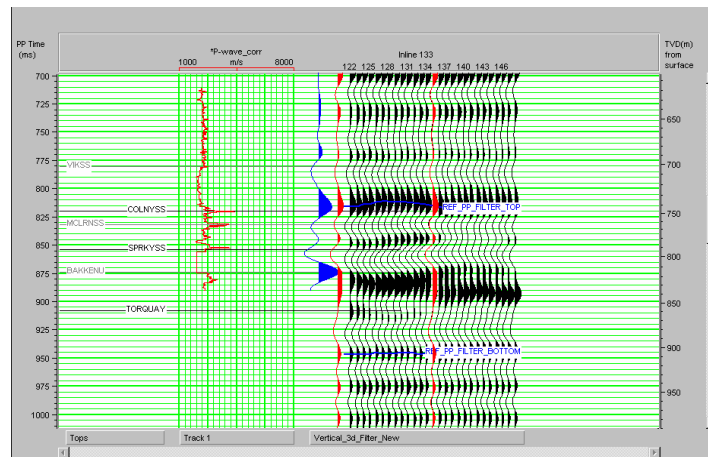


FIG. 4. Synthetics for PP data.

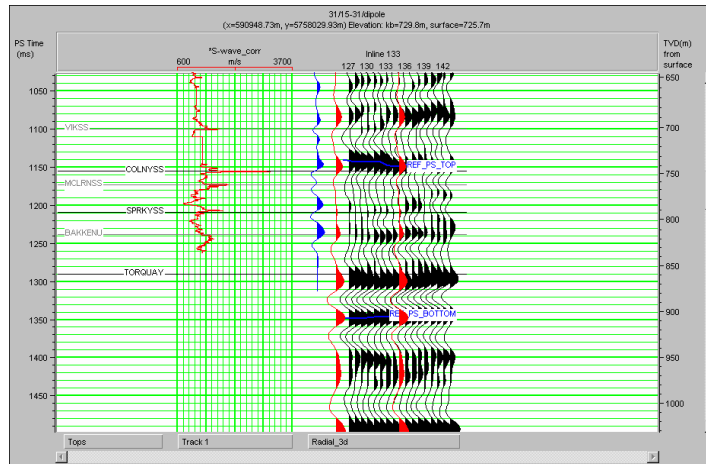


FIG. 5. Synthetics for PS data.

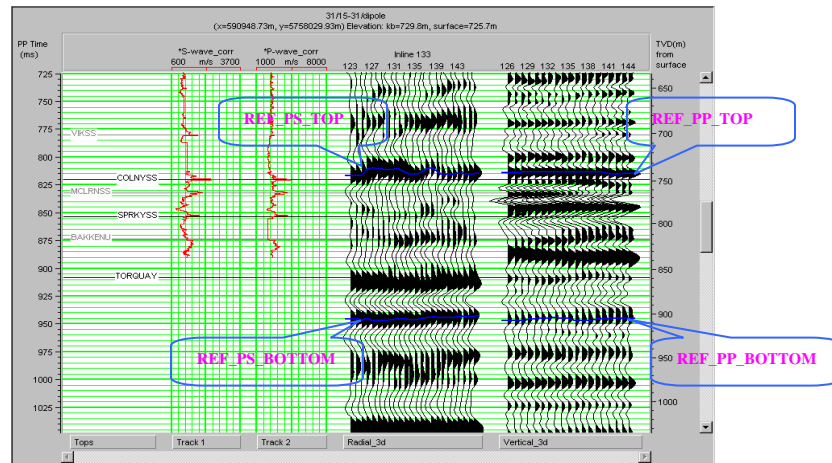


FIG. 6. Selected reference top and bottom horizons.

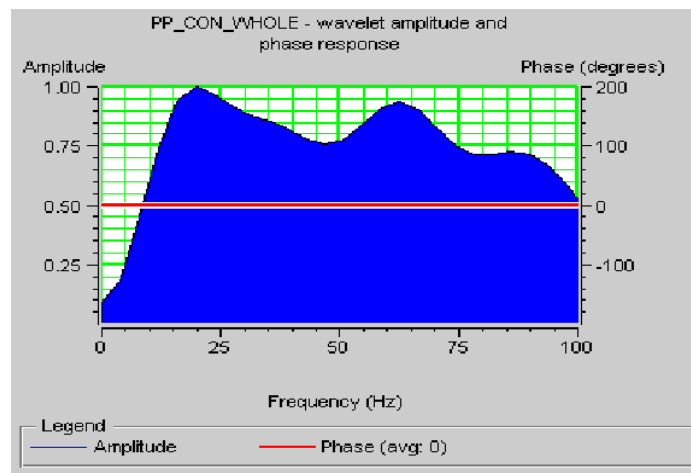


FIG. 7. Amplitude spectrum of PP data.

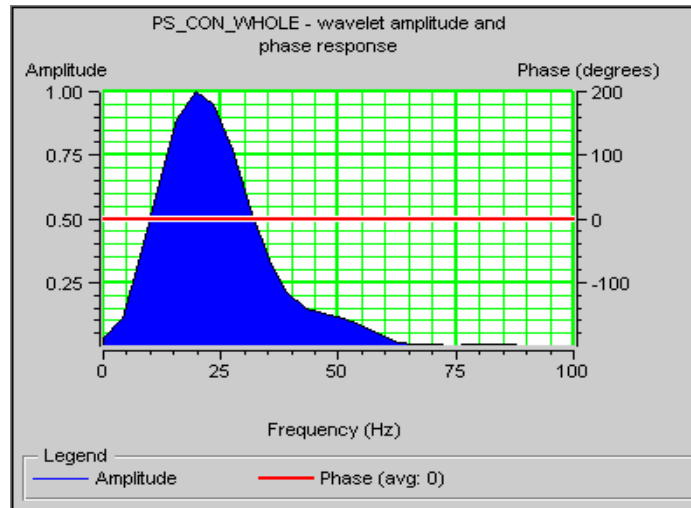


FIG. 8. Amplitude spectrum of PS data.

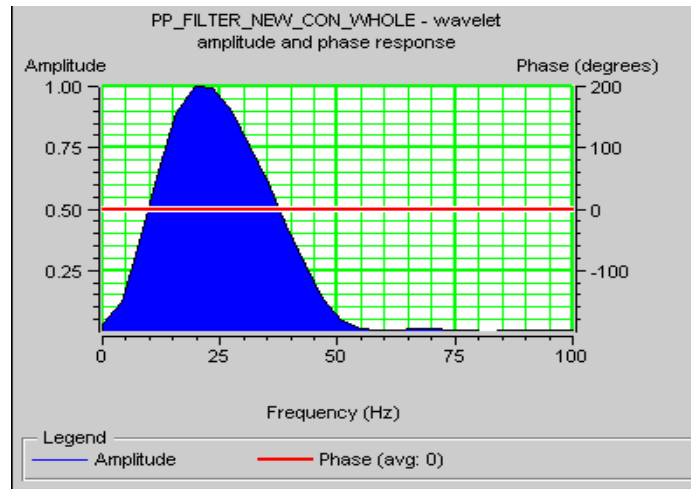


FIG. 9. Amplitude spectrum of filtered PP data.

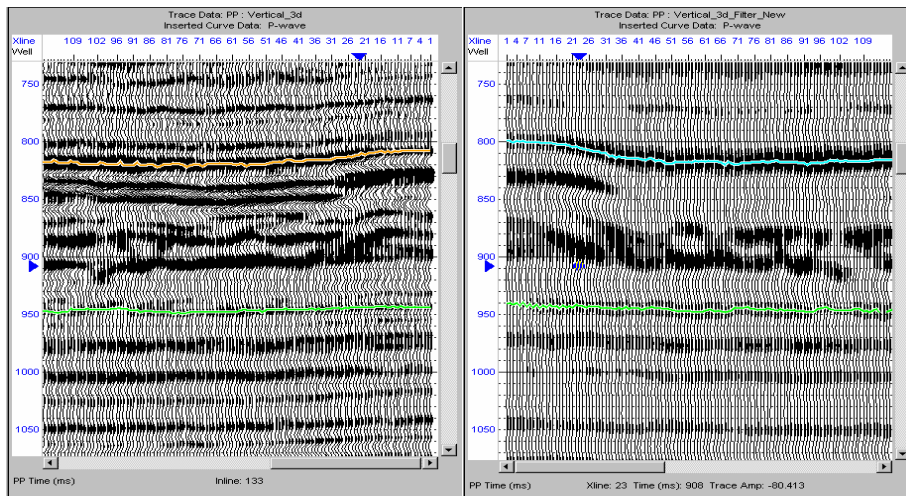


FIG. 10. Comparison between PP (left) and filtered PP (right) data.

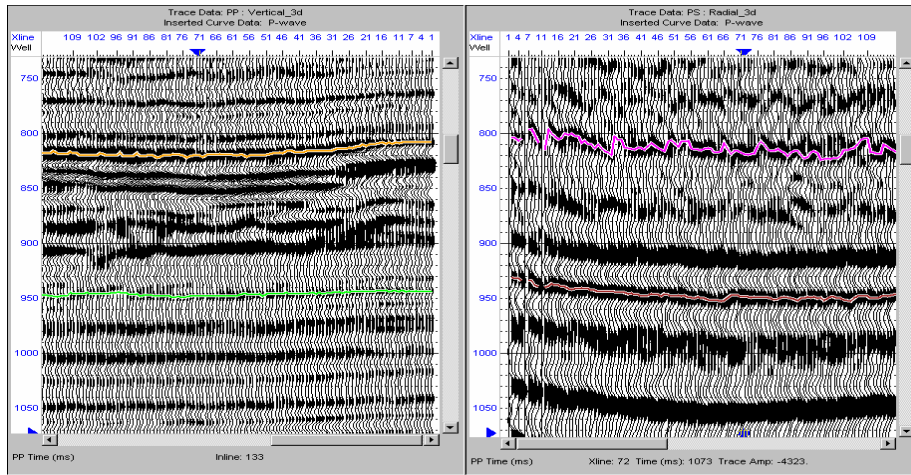


FIG. 11. Comparison between PP (left) and PS (right) data.

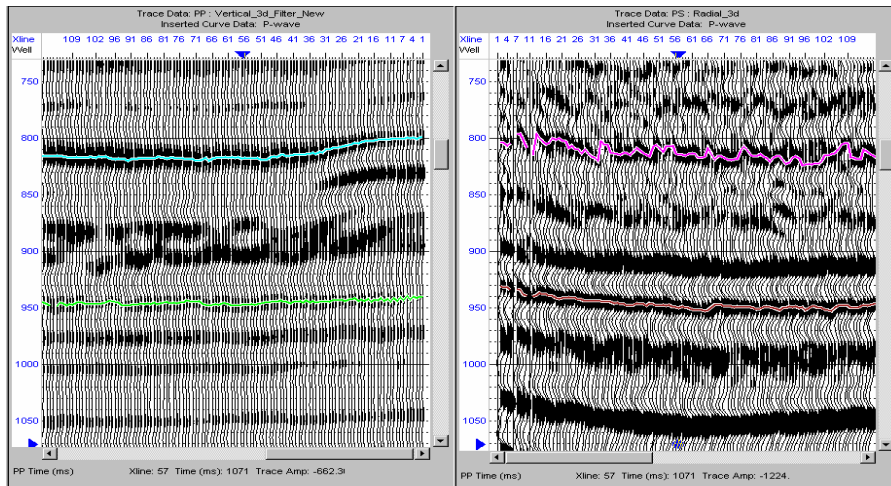


FIG. 12. Comparison between filtered PP (left) and PS (right) data.

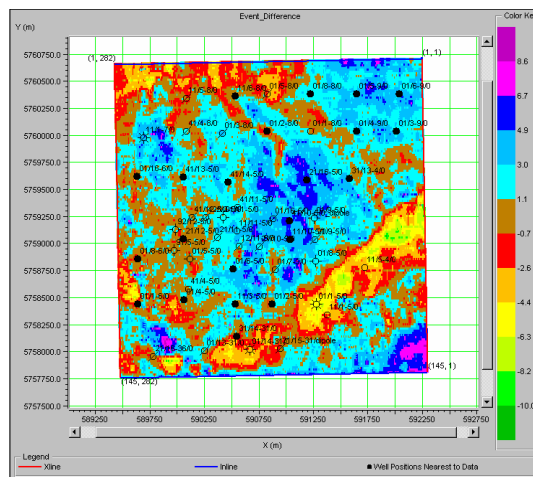


FIG. 13. Difference of top horizons between PP and filtered PP data.

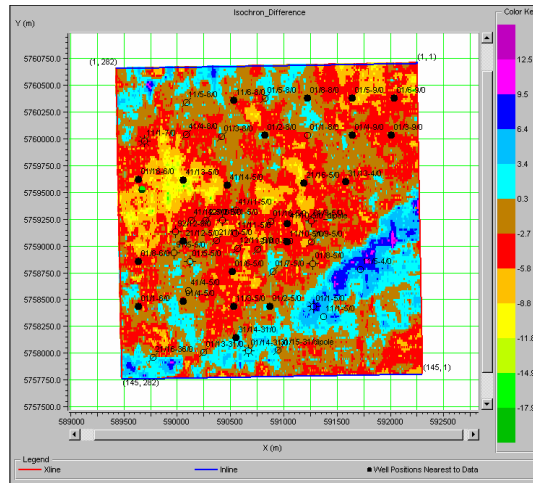


FIG. 14. Difference of isochron maps between PP and filtered PP data.

Some interesting results can be concluded from the isochron maps (Figures 15 and 16). According to the colour legends in these maps, the value of the isochron map from PP data varies between 143 ms and 115 ms, giving a variation of 28 ms; meanwhile, the value from PS data varies from 211 to 193 ms, giving a variation of 18 ms. This means that S-wave travels a longer time in the interpreted interval, but there is less lateral variation of travel time (isochron value) compared with P-wave. In other words, the velocity of P-wave is more sensitive to the environment than S-wave. That is the reason why the pattern of the isochron map from PP data is more colorful than that from PS data. Based on this result, we can make a hypothesis that the velocity of the S-wave shows less variation laterally if the lithology of the interpreted layer doesn't change much.

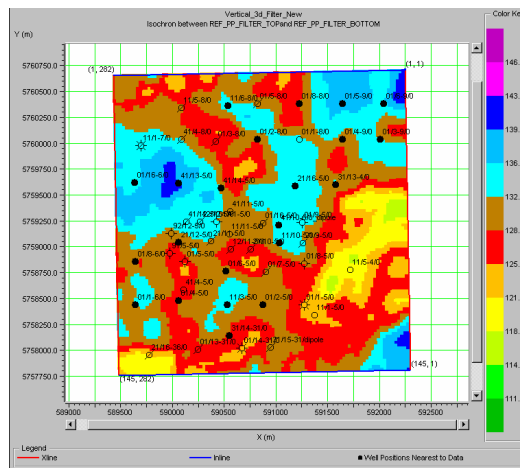


FIG. 15. Isochron map between top and bottom horizons from filtered PP data.

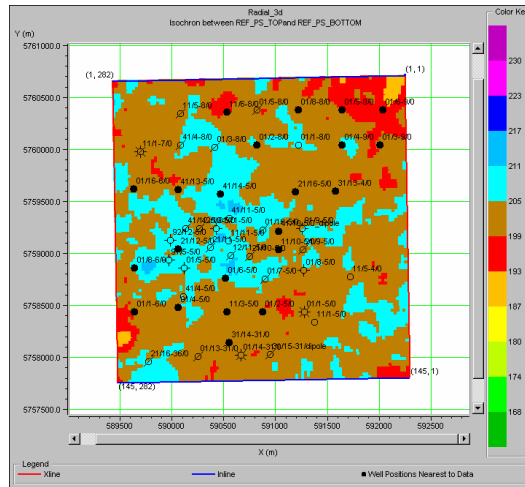


FIG. 16. Isochron map between top and bottom horizons from PS data.

Figures 17 and 18 are the final maps of V_p/V_s between the interpreted reference top and bottom horizons. Yellow, orange and red colors show lower V_p/V_s , most probably deduced by heavy-oil cold production. The values of V_p/V_s around production wells are generally lower than elsewhere. The lower values of V_p/V_s have a good correspondence with well locations in both maps, but the map from filtered PP and PS data has a higher lateral resolution and better correspondence with well locations, especially in the west-center part. This result suggests the importance of the post-stack processing of the seismic volume to enhance the similarity between PP and PS seismic volumes.

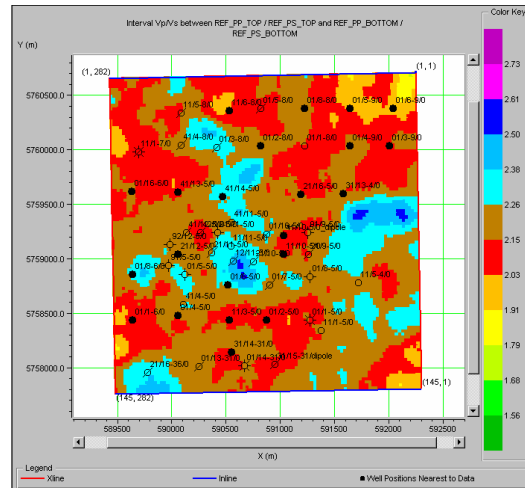


FIG. 17. V_p/V_s between top and bottom horizons from unfiltered PP and PS data.

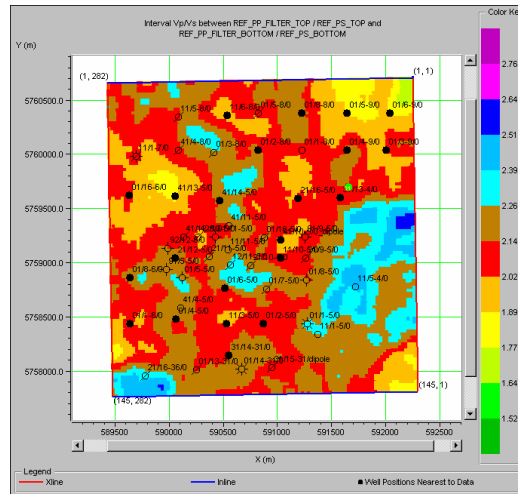


FIG. 18. Vp/Vs between top and bottom horizons from filtered PP and PS data.

ERROR ANALYSIS

Figure 19 is the sketch of the interpreted model of PP and PS data, some parameters are shown in the sketch. If $C_{S1} = \frac{\Delta t_{ps1}}{\Delta t_{ps}}$, $C_{S2} = \frac{\Delta t_{ps2}}{\Delta t_{ps}}$, $C_{P1} = \frac{\Delta t_{pp1}}{\Delta t_{pp}}$, $C_{P2} = \frac{\Delta t_{pp2}}{\Delta t_{pp}}$,

$$\Delta T_{PS} = \Delta t_{ps1} + \Delta t_{ps} + \Delta t_{ps2}, \quad \Delta T_{PP} = \Delta t_{pp1} + \Delta t_{pp} + \Delta t_{pp2}, \quad r_1 = \frac{v_{p1}}{v_{s1}}, \quad r = \frac{v_p}{v_s}, \quad r_2 = \frac{v_{p2}}{v_{s2}},$$

V_p^* is the average velocity of the P-wave between the interpreted interval and V_s^* is the average velocity of the S-wave between the interpreted interval, then the ratio of V_p^* and V_s^* can be expressed as:

$$\begin{aligned}
 R &= \frac{V_P^*}{V_S^*} = \frac{2\Delta T_{PS}}{\Delta T_{PP}} - 1 = \frac{2(\Delta t_{ps1} + \Delta t_{ps} + \Delta t_{ps2})}{\Delta t_{pp1} + \Delta t_{pp} + \Delta t_{pp2}} - 1 \\
 &= \frac{2(C_{S1}\Delta t_{ps} + \Delta t_{ps} + C_{S2}\Delta t_{ps})}{C_{P1}\Delta t_{pp} + \Delta t_{pp} + C_{P2}\Delta t_{pp}} - 1 \\
 &= \frac{C_{S1} + C_{S2} + 1}{C_{P1} + C_{P2} + 1} \frac{v_p}{v_s} + \frac{C_{S1} + C_{S2} - (C_{P1} + C_{P2})}{C_{P1} + C_{P2} + 1}. \tag{2}
 \end{aligned}$$

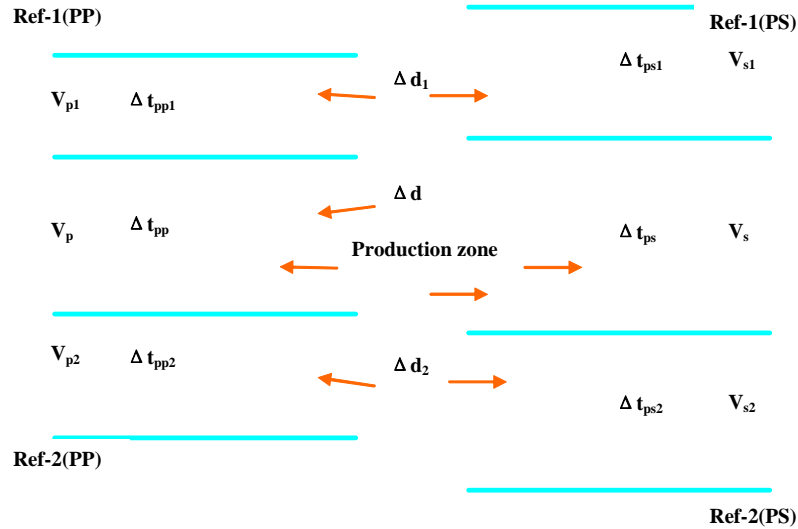


FIG. 19. The sketch of interpreted model.

Since

$$C_{P1} = \frac{\Delta t_{pp1}}{\Delta t_{pp}} = \frac{\Delta d_1}{\Delta d} \frac{v_p}{v_{p1}}, \quad C_{S1} = C_{P1} \frac{\frac{v_{p1}}{v_s} + 1}{\frac{v_p}{v_s} + 1} = C_{P1} \frac{r_1 + 1}{r + 1}, \quad C_{S2} = C_{P2} \frac{r_2 + 1}{r + 1},$$

and then:

$$R = \frac{\frac{r_1 + 1}{r + 1} C_{P1} + \frac{r_2 + 1}{r + 1} C_{P2} + 1}{C_{P1} + C_{P2} + 1} \frac{v_p}{v_s} + \frac{\frac{r_1 + 1}{r + 1} C_{P1} + \frac{r_2 + 1}{r + 1} C_{P2} - (C_{P1} + C_{P2})}{C_{P1} + C_{P2} + 1} \tag{3}$$

If $r_1 \approx r_2 \approx 2.0$, then:

$$R \approx 2 + \frac{r - 2}{C_{p1} + C_{p2} + 1} \quad (4)$$

Assume $\frac{\Delta d_1}{\Delta d} \approx 1$ and $\frac{\Delta d_2}{\Delta d} \approx 1$, then:

$$C_{p1} = \frac{\Delta d_1}{\Delta d} \frac{v_p}{v_{p1}} \approx \frac{v_p}{v_{p1}}, \quad C_{p2} = \frac{\Delta d_2}{\Delta d} \frac{v_p}{v_{p2}} \approx \frac{v_p}{v_{p2}};$$

$$R \approx 2 + \frac{r - 2}{\frac{v_p}{v_{p1}} + \frac{v_p}{v_{p2}} + 1} \quad (5)$$

In a cold production zone, the foamy oil usually has a prominent effect on v_p/v_s and v_p has a dramatic decrease. There will be a large contrast between v_p and v_{p1} or v_{p2} . If we assume $v_{p1} \approx v_{p2}$ (it doesn't matter to our error analysis), then:

$$R \approx 2 + \frac{r - 2}{2 \frac{v_p}{v_{p1}} + 1} = 2 + \frac{r - 2}{2r_p + 1} \quad (6)$$

where $r_p = v_p/v_{p1}$. The error will be:

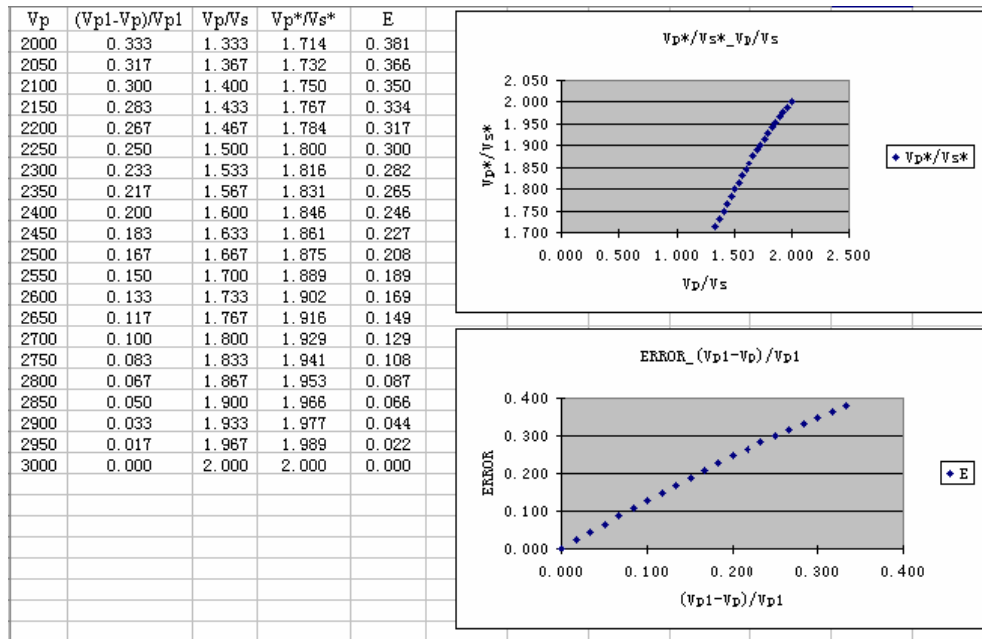
$$E = R - r = (2 - r) \frac{2r_p}{2r_p + 1} \quad (7)$$

The equation of error can be divided into two parts: one is $(2 - r)$, another is $\frac{2r_p}{(2r_p + 1)}$. The first part represents the ratio difference between the production zone and surrounding zone, and 2 is due to our assumption that $r_1 \approx r_2 \approx 2.0$, and the value of this part is the basic element of the error. The second part is actually the coefficient that is due to the difference of the P-wave velocity between the production zone and surrounding zone. Since both r and r_p are variable laterally, the error will be variable laterally.

We assume that: $v_s \approx v_{s1} \approx v_{s2} \approx 1500m/s$ (since v_s doesn't change dramatically due to the presence of foamy oil), $v_{p1} \approx v_{p2} \approx 3000m/s$, based on the above two equations of R and E , the following sheet and graphs are generated. From the sheet and graphs, we

can conclude that: if v_{p1}/v_{s1} and v_{p2}/v_{s2} doesn't change laterally, R will keep the similar pattern with the ratio r of the production zone; but the error will increase with the increasing velocity difference between the production zone and surrounding zone. On the other side, if v_{p1}/v_{s1} and v_{p2}/v_{s2} changes dramatically laterally, then R will probably reach a different pattern compared with r . Thus, generally, we should interpret the reference horizons as close as possible to the top and bottom of the production zone to reduce the effect of the surrounding zone to the least.

Table 3. The error analysis result.



CONCLUSIONS FOR V_p/V_s

Analysis based on the real data interpretation confirmed that V_p is much more sensitive to the reservoir properties compared with V_s . The pattern of V_p/V_s corresponds very well with the locations of the production wells. Post-stack processing of the PP seismic volume to enhance the similarity between PP and PS seismic volumes will generally help us get a more reasonable result. If V_p/V_s of the surrounding zone does not change much laterally, the V_p/V_s calculated from the interpreted interval will correlate with properties of the production zone.

AVO MODELING

As described in the previous part, there are 9 wells available in the area with both P-wave sonic and density well log data, oil well 01/1-6/0 was selected to do AVO modeling. The production zone in this area is about 800 meters deep, and sands are usually poorly consolidated at this depth. Unconsolidated sands are easier to extract simultaneously with

heavy-oil to boost the oil recovery. Gregory (1977) suggested using a value of 0.10 for the dry-rock Poisson's ratio as the additional seed for inverting Gassmann's equation for unconsolidated sands. He noted that σ_{dry} is independent of pressure, and the calculated V_p was not very sensitive to this estimate.

Hilterman (2001) showed that Gassmann's equation can be separated into a dry-rock contribution and a pore-fluid contribution (Figure 20). Two pore-fluid contributions are given: one for water saturation, the other for gas saturation. For the unconsolidated case, the dry-rock contribution (1.63GPa) is only 30% that of the contribution from the fluid (5.51GPa). The choice of pore-fluid saturant dominates the value obtained for V_p . It means that the foamy oil with gas bubbles formed due to decreased pressure will have a detectable effect on V_p . However, the opposite is true for consolidated rocks. The pore-fluid contribution, be it water or gas, contributes little to the rock's total moduli. Accurate estimates of lithology and porosity are important when dealing with consolidated sands.

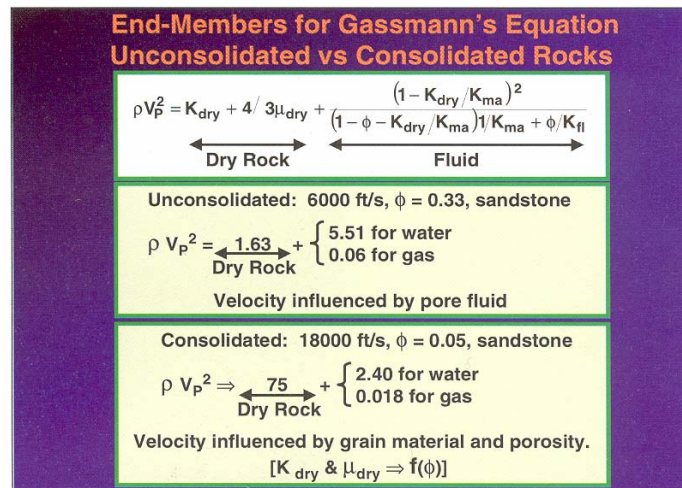


FIG. 20. Separation of Gassmann's equation.

To perform fluid replacement modeling on well data, the basic problem can be formulated as follows: given P-wave velocity and density of a rock and water saturation, derive P-wave and S-wave velocities at different porosities, water saturations and hydrocarbons. In this process, other required parameters are densities and bulk moduli of water, hydrocarbon and matrix solid, and also dry-rock Poisson's ratio (0.12).

According to above description, we know following parameters before production:

V_p : P-wave velocity from well log data;

ρ : density from well log data;

S_{wo} : calculated water saturation from well log data (assumed to be 20%);

σ_{dry} : dry-rock Poisson's ratio (assumed to be 0.12);

ρ_w : density of water (assumed to be default brine: 1.09g/cc);

K_w : bulk modulus of water (assumed to be default brine: 2.38GPa);

ρ_{ho} : density of heavy-oil, calculated based on Batzle-Wang formulas, parameters are shown in Table 1, value is 0.9374g/cc;

K_{ho} : bulk modulus of heavy-oil, value is 0.0524GPa;

ρ_m : weighted average of mineral densities (70% quartz and 30% clay), value is 2.629g/cc;

K_m : Reuss average of mineral bulk moduli, value is 29.87GPa;

μ_m : Reuss average of mineral shear moduli, value is 16.94GPa.

From ρ_w , ρ_{ho} , K_w and K_{ho} , we can get the density (ρ_{who}) and bulk modulus (K_{who}) of total fluid in rock's pore before production:

$$\rho_{who} = S_{wo} * \rho_w + (1 - S_{wo}) * \rho_{ho} = 0.968g/cc \quad (8)$$

$$\frac{1}{K_{who}} = \frac{S_{wo}}{K_w} + \frac{1 - S_{wo}}{K_{ho}} \quad (9)$$

$$K_{who} = 0.0651GPa$$

and the porosity of rock (ϕ) is:

$$\phi = \frac{\rho - \rho_m}{\rho_{who} - \rho_m} \quad (10)$$

The above ϕ is original porosity. After production, the porosity will be improved due to the simultaneous extraction of sand with oil. In this case, the final porosity ϕ^{out} is assumed to be 40%, larger than original porosity.

In the reservoir condition of pressure depletion after heavy-oil cold production, dissolved gas in live heavy-oil comes out of solution as bubbles and trapped within heavy-oil. Both of heavy-oil and trapped bubbles together form the foamy oil, which is a foamy or emulsive state. According to the parameters listed in Table 1, densities and bulk moduli of oil and gas calculated based on Batzle-Wang formulas are:

ρ_h : density of heavy-oil after production, value is 0.8053g/cc;

K_h : bulk modulus of heavy-oil, value is 0.0077GPa;

ρ_g : density of gas after production, value is 0.0101g/cc;

K_g : bulk modulus of gas, value is 0.0021GPa.

If we assume that the foamy oil is composed of 85% oil and 15% gas, density (ρ_f) and bulk modulus (K_f) of foamy oil can be calculated as follows:

$$\rho_f = 0.85 * \rho_h + 0.15 * \rho_g = 0.686 \text{ g / cc} \quad (11)$$

$$\frac{1}{K_f} = \frac{0.85}{K_h} + \frac{0.15}{K_g} \quad (12)$$

$$K_f = 0.0055 \text{ GPa}$$

Further, we can get the density (ρ_{wf}) and bulk modulus (K_{wf}) of total fluid in rock's pore after production (water saturation assumed to keep same with pre-production);

$$\rho_{wf} = S_{wo} * \rho_w + (1 - S_{wo}) * \rho_f = 0.7668 \text{ g / cc} \quad (13)$$

$$\frac{1}{K_{wf}} = \frac{S_{wo}}{K_w} + \frac{1 - S_{wo}}{K_f} \quad (14)$$

$$K_{wf} = 0.00687 \text{ GPa}$$

and total density of fluid and rock (ρ^{out}) after production is:

$$\rho^{out} = \phi^{out} * \rho_{wf} + (1 - \phi^{out}) * \rho_m = 1.884 \text{ g / cc} \quad (15)$$

Actually, the required parameters are well prepared right now, and what we will have to do next is input these parameters in correspondent place when the fluid replacement modeling module (FRM in Hampson-Russell software) is implemented. Those equations used in the Biot-Gassmann's modeling option of AVO program are those given by Gregory (1977) and could be expressed as follows:

In general case, P-wave modulus (M) can be defined as:

$$M = v_p^2 * \rho \quad (16)$$

where Vp and ρ have been given in previous part.

Since the frequencies in seismic records are low, Biot's (1956) theory of wave propagation in the form and notation given by White (1965) can be used and the P-wave modulus (M_{dry}) of the empty skeleton of rock is related to bulk modulus and Poisson's ratio by:

$$M_{dry} = \frac{3(1 - \sigma_{dry})}{1 + \sigma_{dry}} K_{dry} \quad (17)$$

where σ_{dry} is Poisson's ratio of dry rock and is assumed to be 0.12, K_{dry} is bulk modulus of dry rock before production and will be calculated later.

If

$$s = \frac{3(1 - \sigma_{dry})}{1 + \sigma_{dry}}; \quad a = s - 1; \quad b = \phi * s * \left(\frac{K_m}{K_{who}} - 1\right) - s + \frac{M}{K_m};$$

$$c = -\phi * \left(s - \frac{M}{K_m}\right) * \left(\frac{K_m}{K_{who}} - 1\right); \quad y = 1 - \frac{K_{dry}}{K_m}$$

then, y can be solved using quadratic equation:

$$ay^2 + by + c = 0 \quad (18)$$

and then:

$$y = \frac{-b + \sqrt{b^2 - 4ac}}{2a} \quad (19)$$

where ϕ , K_m , K_{who} and M have been given or calculated in previous part.

From y , we can get K_{dry} :

$$K_{dry} = K_m * (1 - y) \quad (20)$$

and then:

$$\mu_{dry} = \mu = 3(1 - 2\sigma_{dry}) \frac{K_{dry}}{2(1 + \sigma_{dry})} \quad (21)$$

where μ_{dry} and μ are shear moduli of dry rock and saturated rock.

To calculate bulk modulus of dry rock at new porosity values after production, a new parameter, pore bulk modulus (K_ϕ) is defined:

$$\frac{\phi}{K_\phi} = \frac{1}{K_{dry}} - \frac{1}{K_m} \quad (22)$$

and then:

$$\frac{1}{K_{dry}^{out}} = \frac{\phi^{out}}{K_\phi} + \frac{1}{K_m} \quad (23)$$

where K_{dry}^{out} is bulk modulus of dry rock at new porosity value ϕ^{out} .

From K_{dry}^{out} , we can calculate shear moduli at new porosity value:

$$\mu_{dry}^{out} = \mu^{out} = 3(1 - 2\sigma_{dry}) \frac{K_{dry}^{out}}{2(1 + \sigma_{dry})} \quad (24)$$

where μ_{dry}^{out} and μ_{dry} are shear moduli of dry rock and saturated rock at new porosity value after production.

Right now, all required parameters to calculate velocities of P-wave and S-wave at new situation using Biot-Gassmann's equation are prepared, it's time to get v_p^{out} and v_s^{out} .

If

$$n = \left(1 - \frac{K_{dry}^{out}}{K_m}\right)^2; \quad d = \frac{\phi^{out}}{K_{wf}} + \left(1 - \frac{\phi^{out}}{K_m} - \frac{K_{dry}^{out}}{K_m^2}\right)$$

then P-wave modulus (M^{out}) at new situation is:

$$M^{out} = s * K_{dry}^{out} + \frac{n}{d} \quad (25)$$

and then:

$$v_p^{out} = \sqrt{\frac{M^{out}}{\rho^{out}}} \quad (26)$$

$$v_s^{out} = \sqrt{\frac{\mu^{out}}{\rho^{out}}} \quad (27)$$

SYNTHETICS AND INTERPRETATION

Based on parameters calculated in previous part, synthetic seismograms were created for wet condition, pre-production and post-production respectively (Figure 21). All synthetics are displayed with reversed polarity. The picked event is from top of pay zone.

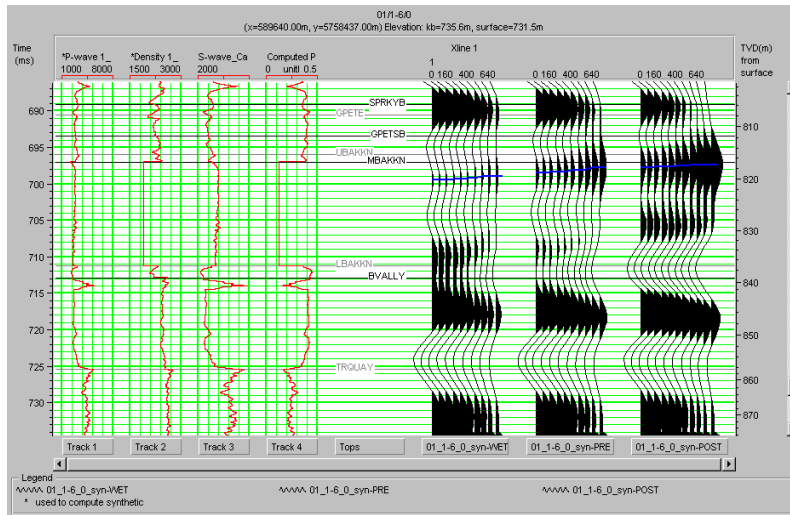


FIG. 21. AVO synthetics for well 01/1-6/0.

In Figure 21, left synthetics are for the wet condition, water saturation S_w is assumed to be 100%, the amplitude of reflection is weakest. Middle synthetics are for pre-production, heavy-oil saturation is assumed to be 80%, water saturation is assumed to be 20%, the amplitude of reflection from the top of pay zone is stronger than that in wet condition. Right synthetics are for post-production, porosity is assumed to be improved to 40% due to the forming of wormhole, water saturation is the same and heavy-oil is changed to foamy oil due to pressure drop and coming out of dissolved gas. Obviously, the reflection amplitude is strongest and the magnitude is improved with offset. The above results are easier to discriminate in Figure 22, in which the yellow curve represent the amplitude of picked event from synthetics for wet condition; the blue curve represent the amplitude of picked event from synthetics for pre-production; the red curve represent the amplitude of picked event from synthetics for post-production. This is a typical Class III AVO response.

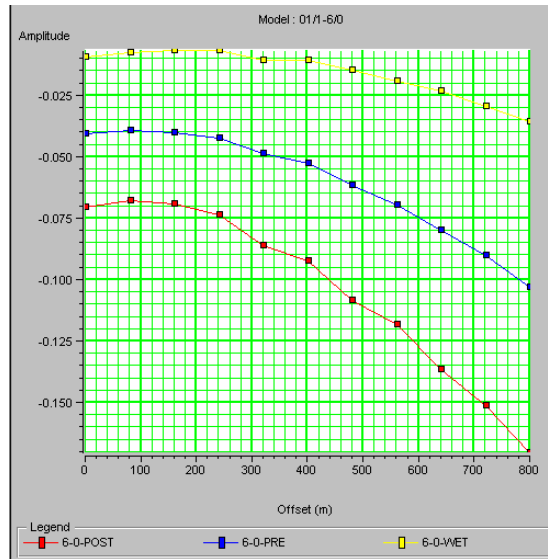


FIG. 22. AVO curves for well 01/1-6/0.

Since this is a typical Class III AVO response, A^*B can be used to indicate the pay zone (Figure 23), where A is inverted intercept and B is inverted gradient from synthetic seismograms. In the figure, traces 1-6 represent wet case, 7-12 represent pre-production situation, 13-18 represent post-production. A^*B value of post-production in the pay zone is obviously distinguished from the other two cases. The large red anomaly at the zone of interest on the post-production traces is not present on the pre-production traces. A^*B is very good at differentiating post-and pre-production reservoir condition.

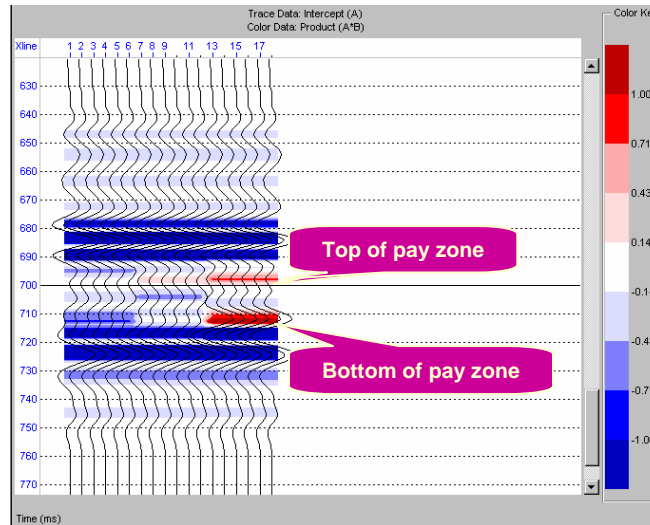


FIG.23 AVO attribute (A^*B).

CONCLUSIONS FOR AVO ANALYSIS

In unconsolidated sand reservoirs, cold production of heavy-oil will create a typical Class III AVO response. The indicator A^*B value of post-production from pay zone is obviously distinguished from other cases.

ACKNOWLEDGEMENTS

We would like to thank Joan Embleton, Kevin Hall, Rolf Maier, Richard Xu and Bruce Palmiere for their support and technical discussions. I am also grateful to the sponsors for their support to the CREWES and CHORUS projects.

REFERENCES

- Batzle, M., and Wang, Z., 1992, Seismic properties of pore fluids, *Geophysics*, **57**, 1396-1408.
- Castagna, J. P., and Smith, S. W., 1994, Comparison of AVO indicators: A modeling study, *Geophysics*, **59**, 1849-1855.
- Chen, S., Lines, L., Embleton, J., Daley, P.F. and Mayo, L., 2003, Seismic detection of cold production footprints of heavy oil in Lloydminster field, the CSEG convention, June, Calgary, Alberta, Canada.
- Domenico, S. N., 1974, Effect of water saturation on seismic reflectivity of sand reservoirs encased in shale, *Geophysics*, **39**, 759-769.
- Gregory, A.R., 1977, Aspects of rock physics from laboratory and log data that are important to seismic interpretation, *AAPG memoir* **26**, 15-46.
- Hampson, D., and Russell, B., 2003, *Manual of Hampson-Russell software: AVO*.

- Hilterman, F. J., 2001, Seismic amplitude interpretation, Short Course, SEG, Distinguished Instructor Series, No.4.
- Lines, L., Chen, S., Daley, P.F., Embleton, J. and Mayo, L., 2003, Seismic pursuit of wormholes, *The Leading Edge*, **22**, 459-461.
- Lines, L. R., Zou, Y., Zhang, D. A., Hall, K., Embleton, J., Palmiere, B., Reine, C., Bessette, P., Cary, P., and Secord, D., 2005, V_p/V_s characterization of a heavy-oil reservoir, *The Leading Edge*, 24.
- Murphy, W., Reischer, A., and Hsu, K., 1993, Modulus decomposition of compressional and shear velocities in sand bodies, *Geophysics*, **58**, 227-239.
- Rutherford, S. R., and Williams, R.H., 1989, Amplitude-versus-offset in gas sands, *Geophysics*, **54**, P680-688.
- Sawatzky, R.P., Lillico, D.A., London, M.J., Tremblay, B.R. and Coates, R.M., 2002, Tracking cold production footprints, CIPC conference, Calgary, Alberta, Canada.
- Watson, I. A., Lines, L. R., and Brittle, K. F., 2002, Heavy-oil reservoir characterization using elastic wave properties, *The Leading Edge*, **21**, 736-739.